RSC Advances

PAPER

View Article Online
View Journal | View Issue

Cite this: *RSC Adv.*, 2020, **10**, 24808

Lanthanide complexes based on a new bis-chelating carbacylamidophosphate (CAPh) scorpionate-like ligand†

Iryna Olyshevets, *[a] Vladimir Ovchynnikov,[a] Nataliia Kariaka,[a] Viktoriya Dyakonenko,[b] Svitlana Shishkina,[b] Tatiana Sliva,[a] Małgorzata Ostrowska,[c] Aleksandra Jedyńczuk,[c] Elżbieta Gumienna-Kontecka[c] and Vladimir Amirkhanov[a]

Received 28th May 2020
Accepted 19th June 2020

DOI: 10.1039/d0ra04714g

rsc.li/rsc-advances

The novel bis-chelating carbacylamidophosphate type ligand, tetramethyl[pyridine-2,6-diyldi(iminocarbonyl)] diamidophosphate (H_2L), and its sodium salt, NaHL, have been synthesized and their structural properties have been investigated. Coordination compounds of lanthanides $[Ln(HL)_2NO_3]\cdot$i-PrOH (Ln = Eu^{3+}, Tb^{3+}) were obtained for the first time, isolated in the individual state and characterized by means of IR and NMR spectroscopies, electrospray ionization mass spectrometry (ESI-MS), potentiometric titration, and elemental, thermal gravimetric and X-ray diffraction analyses. It was shown that H_2L behaves like a scorpionate type ligand and in a mono-deprotonated form coordinates in a tridentate manner *via* the oxygen atoms of phosphoryl and carbonyl groups with formation of a mononuclear metal complex. The protonation constants of H_2L and stability constants of Eu^{3+} and Tb^{3+} complexes have been determined. According to the results of X-ray diffraction analysis the H_2L and $[Ln(HL)_2NO_3]\cdot$i-PrOH molecules have monomeric structure but NaHL is a dimer. The Hirshfeld surface and fingerprint plots of the compounds have been used to analyze various hydrogen bonds and intermolecular interactions displayed in the crystal structure.

Introduction

Recently, the research of coordination compounds of lanthanides has been intensively developing, which is associated with the prospect of their practical application in the latest technologies, biology and medicine.[1] Because of numerous unique physical properties of lanthanide containing compounds, including the ability of lanthanide complexes to radiate in a rather narrow spectral range, a large number of studies have been aimed at creating new luminescent materials on their basis.[2] Lanthanide based complexes can also be used in medicine as contrast agents for MRI trials,[3] luminescent probes[4] *etc.*

Over the past decades, many papers have been devoted to the use of lanthanide complexes in the technology of organic electroluminescent diodes (OLED),[2a,5] a large part of which involves the study of β-diketonate complexes of lanthanides with "antenna" ligands, capable of transforming light energy from the UV region into the visible one due to excitation of f-electrons.[6] Lanthanide complexes with P, N-hetero-substituted structural analogues of β-diketones – carbacylamidophosphates (CAPh) – compounds containing the chelating fragment C(O)NHP(O) – have some essential advantages.[7] The presence of a phosphorus atom in the functional fragment provides synthetic possibilities (compared with β-diketones) for the introduction of additional functional groups-antenna. Moreover, compared with β-diketones, replacing one of the C=O groups with the P=O group in the CAPh ligands leads to a decrease of vibration energy of Ln^{3+} coordinated fragments (from ~1600 cm^{-1} to ~1250 cm^{-1}) and replacement of the carbon atom of chelating moiety with nitrogen one eliminates high-frequency C–H vibrations in chelating ring. These factors decrease the multiphoton quenching of the lanthanide emission in Ln^{3+} CAPh based complexes.

The compounds of the bis-β-diketonate series are promising chelating ligands, and their complexes with lanthanide ions have excellent photoluminescence properties[6b,8] and can be used as markers in various variants of time-resolved fluorescence analysis. The syntheses of chelates based on bis-β-diketones are rather cheap and have high yields; also rather high stability constants of such complexes allow conducting measurements on the solid phase and in solution. β-Diketonate

[a]*Taras Shevchenko National University of Kyiv, Department of Chemistry, 64/13, Volodymyrska Street, Kyiv 01601, Ukraine. E-mail: olishevetsirina@gmail.com*

[b]*Institute for Single Crystals, National Academy of Science of Ukraine, Nauky ave. 60, Kharkiv 61001, Ukraine*

[c]*Faculty of Chemistry, University of Wroclaw, F. Joliot-Curie 14, Wroclaw, 50383, Poland*

† Electronic supplementary information (ESI) available. CCDC 1984336–1984339. For ESI and crystallographic data in CIF or other electronic format see DOI: 10.1039/d0ra04714g

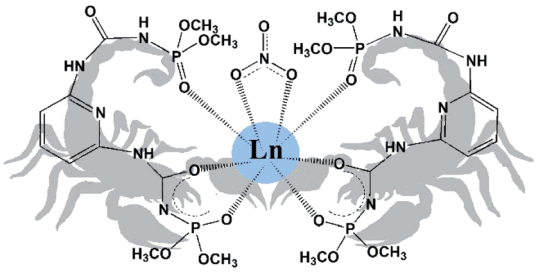

Fig. 1 Schematic representation of obtained scorpionate complexes $[Ln(HL)_2NO_3]\cdot$i-PrOH (2-propanol molecule is omitted).

type complexones are also used for the detection of rare-earth elements, their extraction and concentration.[9]

Another promising type of ligands is "scorpionates". Scorpionate ligands are the tridentate ligands which bind to a metal in a fac-manner. As an example, among the most popular class of scorpionates one can mention the pyrazol-based borates.[10] The advantage of scorpionate complexes is that their easily tuneable electronic and steric features lead to the formation of very stable complexes with interesting and unique properties.[11] As it will be shown in this research, the monodeprotonated bis-chelating CAPh ligand, due to its specific steric structure, behaves like a scorpionate ligand binding a metal by two oxygen atoms of deprotonated chelating core, like the pincers of a scorpion, and by the third oxygen atom of phosphoryl group of non-deprotonated arm of the ligand, which is situated over the plane formed by the metal and the two donor oxygen atoms of deprotonated chelating core (Fig. 1).

In this paper we report synthesis, structures, spectral and thermal properties of new bis-CAPh type ligand tetramethyl [pyridine-2,6-diyldi(iminocarbonyl)]diamidophosphate ($\mathbf{H_2L}$), it's sodium salt, and europium(III) and terbium(III) complexes of general formula $\mathbf{[Ln(HL)_2NO_3]}\cdot$i-PrOH.

Experimental section

Materials and methods

All of the chemicals used in this work were of analytical grade and used without further purification. Solutions of NaOH, HCl, NaCl, $Eu(NO_3)_3\cdot 6H_2O$, and $Tb(NO_3)_3\cdot 6H_2O$ were prepared from pure commercial products (Sigma Aldrich). Stock solutions were standardized by ICP-AES along with the complexometric titration against EDTA using xylenol orange as an indicator. HCl solution was titrated by standardized NaOH solution. Carbonate-free NaOH solution was standardized by titration with potassium hydrogen phthalate.

IR measurements were performed on a Perkin-Elmer Spectrum BX spectrometer on samples in form of KBr pellets.

^{1}H NMR spectra in DMSO-d_6 solutions were obtained on an AVANCE 400 Bruker NMR spectrometer at room temperature.

Elemental analyses (C, H, N) were performed on an EL III Universal CHNOS Elemental Analyzer.

Thermal gravimetric analysis was performed using a synchronous TG/DTA analyzer Shimadzu DTG-60H. The typical sample of 5–10 mg was heated to 800 °C in the alumina crucible under steady argon flow (300 ml min^{-1}), with the heating rate of 10 °C min^{-1}. The crystalline powdery Al_2O_3 was used as a standard compound.

X-ray diffraction data for structures $\mathbf{H_2L}$, $\mathbf{NaHL}\cdot$i-PrOH and $\mathbf{[Ln(HL)_2NO_3]}\cdot$i-PrOH (Ln = Eu^{3+}, Tb^{3+}) were collected on an Xcalibur-3 diffractometer (graphite monochromated MoK_α radiation, CCD detector, φ and ω-scanning). The structures were solved by direct method and refined against F^2 by full-matrix least-squares method using the SHELXTL package.[12] All non-hydrogen atoms were refined within anisotropic approximation. The H atoms were located from the electron density difference maps and refined by "riding" model with $U_{iso} = nU_{eq}$ of the carrier atom (n = 1.5 for methyl and hydroxyl groups and n = 1.2 for other hydrogen atoms). The crystal and structure refinement data for $\mathbf{H_2L}$, $\mathbf{NaHL}\cdot$i-PrOH and $\mathbf{[Ln(HL)_2NO_3]}\cdot$i-PrOH (Ln = Eu^{3+}, Tb^{3+}) are given in Table S1.† Final atomic coordinates, geometrical parameters and crystallographic data have been deposited into the Cambridge Crystallographic Data Center, 11 Union Road, Cambridge, CB2 1EZ, UK (E-mail: deposit@ccdc.cam.ac.uk; fax: +44 1223 336033).

Electrospray ionization mass spectrometry (ESI-MS) data were recorded on a BrukerQ-FTMS spectrometer. The instrumental parameters were: scan range, m/z 200–1600; dry gas, nitrogen; temperature, 170 °C; capillary voltage, 4500 V; ion energy, 5 eV. The capillary voltage was optimized to the highest signal-to-noise ratio. The spectra were recorded in the positive negative ion modes. MeOH/H_2O solvent (50/50 v/v) was used to prepare solutions of ligand with concentrations of 10^{-4} to 10^{-5} M and metal-to-ligand molar ratios 1 : 1 and 1 : 3 with pH 3 and 8.

The potentiometric titrations were performed at a constant temperature of 25 °C in an atmosphere of argon as an inert gas, using an automatic titrator system Titrando 905 (Methrom), connected to a combined glass electrode (Mettler Toledo InLab Semi-Micro) calibrated daily for hydrogen ion concentration using HCl. All the titrations were performed on 0.1 M solutions, using NaCl as a background electrolyte. Starting volumes of *ca.* 2 mM ligand solutions were 3 ml, and the exact concentration of the ligand was determined using the method of Gran.[13] Metal-to-ligand molar ratios were 1 : 1 and 1 : 3 for all metal ions. The potentiometric data, collected over a pH range 2.0–11.0, were refined with the SUPERQUAD[14] program, which use nonlinear least-squares methods. The species distribution diagrams were generated using a computer HYSS program.[15]

The three-dimensional Hirshfeld surfaces (HSs) and two-dimensional fingerprint plots were generated using Crystal Explorer 3.0.[16,17] The d_{norm} plots were mapped with color scale in between – 0.649 au (blue) and 1.554 au (red). The fingerprint plots were displayed by using the expanded 0.4–2.4–3.0 Å view with the d_e and d_i distance scales displayed on the graph axes. When the *cif* files were uploaded into the CrystalExplorer software, all bond lengths to hydrogen were automatically modified to typical standard neutron values, *i.e.*, d(C–H) = 1.083 and d(O–H) = 0.983 Å.

Synthetic procedures

Synthesis of $\mathbf{H_2L}$. $\mathbf{H_2L}$ compound was synthesized for the first time according to general procedure described previously.[7a]

0.018 mol of 2,6-diaminopyridine was dissolved in 40 ml of dioxane. The mixture was added dropwise to a solution of 0.036 mol of dimethyl ester of isocyanatophosphate acid in 40 ml of diethyl ether, with vigorous stirring and cooling. Yield 80%, M.P. = 155 °C. The compound is soluble in alcohols, acetone and water.

Compound ***H_2L.*** Analysis for $C_{11}H_{19}N_5O_8P_2$, %: calculated – C 32.13, H 4.66, N 17.02; found – C 32.41, H 4.36, N 16.98.

IR (KBr pellet, cm^{-1}): 1689, 1729 (ν(C═O)), 1256 (ν(P═O)).

^{1}H NMR (400 MHz, DMSO-d_6, 25 °C): d = 3.69–3.72 (d, 12H, 3 J P-H = 11.5 Hz, OCH_3), 7.40 (d, 2Hb, C_5H_3N), 7.71 (t, 1Hc, C_5H_3N), 8.8 (s, 2H, NH(CO)), 9.25 (s, 2H, NH(P)).

Synthesis of NaHL·i-PrOH. The sodium salt **NaHL** was prepared by the reaction between $\mathbf{H_2L}$ and 1 equivalent of sodium methanolate in methanol. The resulting solution was evaporated and the fine-crystalline powder was isolated (yield 90%). The single crystals of the compound **NaHL**·i-PrOH were obtained by slow evaporation from its solution in 2-propanol. The compound is soluble in methanol, propanol-2, acetone and water.

Compound ***NaHL.*** Analysis for $C_{11}H_{18}NaN_5O_8P_2$, %: calculated – C 30.50, H 4.20, N 16.17; found – C 30.44, H 4.11, N 16.19.

IR (KBr pellet, cm^{-1}): 1606, 1699 (ν(C═O)), 1223 (ν(P═O)).

^{1}H NMR (400 MHz, DMSO-d6, 25 °C): d = 3.61–3.64 (d, 12H, 3 J P–H = 11.5 Hz, OCH_3), 7.05 (d, 2Hb, C_5H_3N), 7.50 (t, 1Hc, C_5H_3N), 8.8 (s, 2H, NH(CO)), 9.23 (s, 1H, NH(P)).

Synthesis of $[Ln(HL)_2NO_3]$·i-PrOH (Ln = Eu, Tb). Hydrated Ln(III) nitrate (1 mmol) was dissolved in 2-propanol (15 ml) and added to the solution of **NaHL** (2 mmol) in 15 ml of acetone. The resulted mixture was boiled for some minutes and then cooled to the room temperature. After 15 min the precipitated $NaNO_3$ was filtered off. The resulting clear solution was left at ambient temperature in desiccator over anhydrous $CaCl_2$. In a day the coordination compound precipitated as powder and was filtered off, washed with cold isopropanol and finally dried on air. Yield of the complexes was 70% and 90%, respectively.

Analysis for $C_{25}H_{44}N_{11}O_{20}P_4Eu$, %: calculated – C 27.43, H 4.05, N 14.08; found – C 27.01, H 4.13, N 14.12. IR (KBr pellet, cm^{-1}): 1556, 1652 (ν(C═O)), 1215 (ν(P═O)), 1299, 1507 (NO_3^-).

Analysis for $C_{25}H_{44}N_{11}O_{20}P_4Tb$, %: calculated – C 27.26, H 4.03, N 13.99; found – C 27.41, H 4.13, N 14.02. IR (KBr pellet, cm^{-1}): 1556, 1650 (ν(C═O)), 1190 (ν(P═O)), 1299, 1507 (NO_3^-).

They are soluble in water, methanol, soluble poorly in 2-propanol, acetone, DMSO and insoluble in nonpolar aromatic solvents.

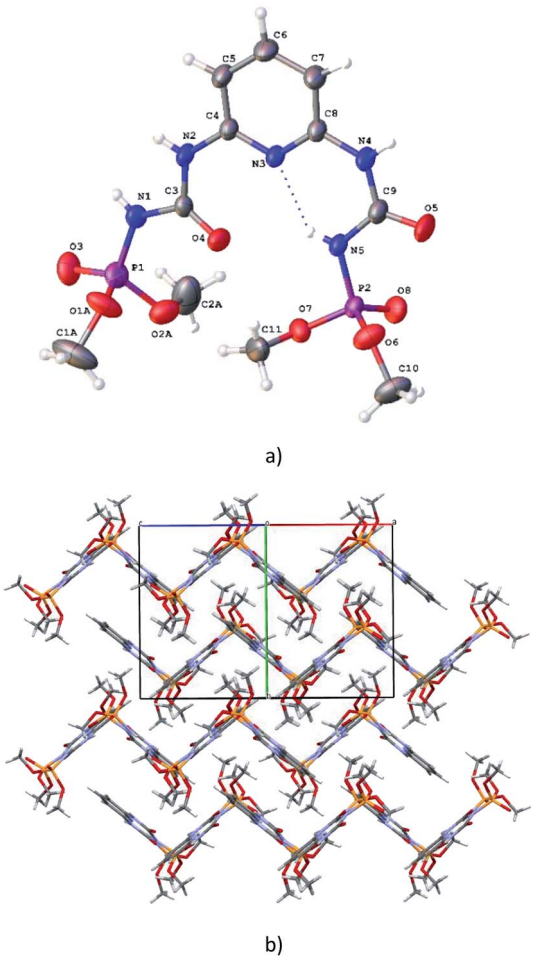

Fig. 2 Molecular (a) and crystal (b) structures of tetramethyl[pyridine-2,6-diyldi(iminocarbonyl)]diamidophosphate (H_2L).

Results and discussion

Description of the crystal structure

Molecular and crystal structure of H_2L. The $\mathbf{H_2L}$ molecule has the pyridine cycle substituted in meta-position to each other by the same substituents with slightly different conformation (Fig. 2a). The phosphoryl and carbonyl groups are turned to each other in synclinal way in one substituent and have anti-periplanar orientation in the other substituent (the corresponding O═C···P═O pseudo-torsion angles are −55.8(1)° and −162.8(1)°). The both of these conformations are characteristic for CAPh.[7a] It should be noted that orientation of two

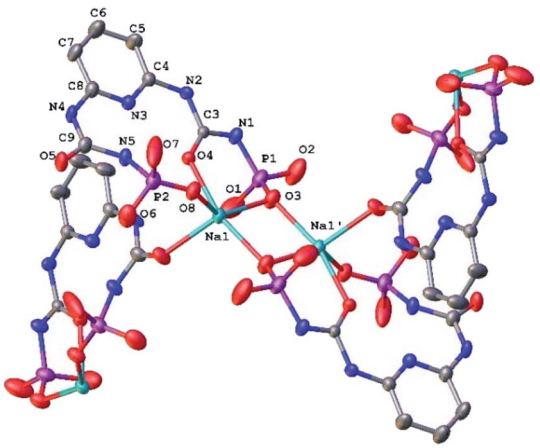

Fig. 3 The fragment of molecular structure of NaHL·i-PrOH (H-atoms and CH_3 of methoxy groups are omitted for clarity; the numbering scheme is given for the asymmetrical part of the unit cell).

substituents in $\mathbf{H_2L}$ are stabilized additionally by the N5–H⋯N3/O4 bifurcated intramolecular hydrogen bonds (Table S3†). The bond lengths of the chelating fragments are d(PO)*syn* = 1.458(2) Å, d(CO)*syn* = 1.226(2) Å, d(PO)*anti* = 1.456(1) Å, d(CO)*anti* = 1.203(1) Å (Table S2†). In the crystal phase $\mathbf{H_2L}$ molecules are bind by the N–H⋯O intermolecular hydrogen bonds (Table S3†) forming corrugated layers parallel to the *ac* crystallographic plane (Fig. 2b).

Molecular and crystal structure of NaHL·i-PrOH. Sodium salt of tetramethyl[pyridine-2,6-diyldi(iminocarbonyl)] diamidophosphate exists as polymer with propanol solvate molecules in the crystal phase (Fig. 3). Only one substituent is deprotonated in the organic ligand but all the carbonyl and phosphoryl oxygen atoms of both substituents participate in coordination of the sodium atom. At that the sodium atom is coordinated by five oxygen atoms belonging to three CAPh ligands and its coordination polyhedron is the distorted trigonal bipyramid. One of these ligands coordinates the sodium atom in tridentate (scorpionate) manner through both carbonyl and phosphoryl oxygen atoms of the deprotonated substituent as well as phosphoryl group oxygen atom of neutral substituent. And the other two ligands coordinate the sodium atom in monodentate manner through the carbonyl group oxygen atom of the neutral substituent or the phosphoryl group oxygen atom of the deprotonated substituent. It should be noted that the phosphoryl group oxygen atom of the deprotonated substituent is bridged between two sodium atoms (Fig. 3).

The Na–O bond lengths in the coordination polyhedron vary within 2.265(4) ÷ 2.400(4) Å and the O–Na–O bond angles vary within 79.15(2) ÷ 103.28(1)° and 95.97(2) ÷ 137.70(1)° in the axial and equatorial directions, respectively (Table S2†).

The bond lengths and bond angles of the **NaHL** ligand are in good agreement with the values for the free ligand (Table S2†). But the conformations of both substituents are changed due to rotation of both dimethoxyphosphoryl groups around the N–P bonds (Fig. 3). The N5–H⋯N3/O4 bifurcated intramolecular hydrogen bonds are very close to ones in the free ligand $\mathbf{H_2L}$ (Table S3†).

In the crystal phase, $(\mathbf{NaHL})_n$ polymeric chains and isopropanol solvent molecules form the alternating layers parallel to the *bc* crystallographic plane (Fig. 4). The ligand molecule and propanol solvate molecules are bind by N–H⋯O and O–H⋯N intermolecular hydrogen bonds (Table S3†).

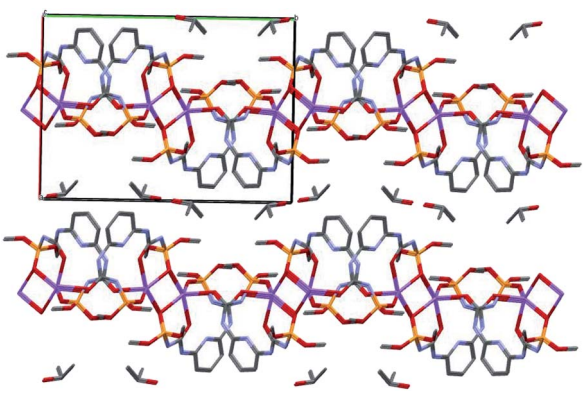

Fig. 4 The crystal packing of $(\mathbf{NaHL}\cdot$i-PrOH$)_n$, projection along the *c* crystallographic direction. H-atoms are omitted for clarity.

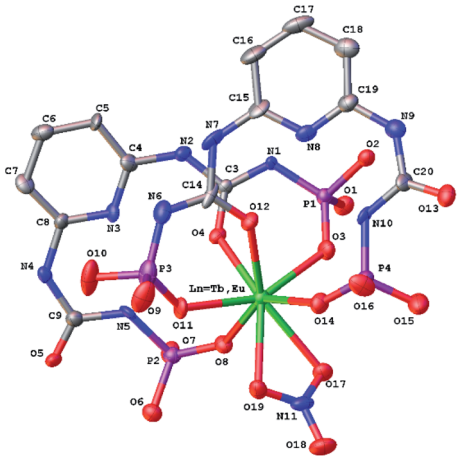

Fig. 5 Molecular structure of $[\mathbf{Ln(HL)_2(NO_3)}]$ (Ln = Eu^{3+}, Tb^{3+}) (H-atoms and CH_3 of methoxy groups are omitted for clarity).

Molecular and crystal structure of $[\mathbf{Ln(HL)_2NO_3}]\cdot$i-PrOH (Ln = $\mathbf{Eu^{3+}}$, $\mathbf{Tb^{3+}}$). The coordination compounds $[\mathbf{Ln(HL)_2(NO_3)}]\cdot$i-PrOH (where Ln = Eu^{3+}, Tb^{3+}) have monomeric structures and are isostructural to each other. In both structures, two deprotonated $\mathbf{HL^-}$ ligands coordinates Ln atom in scorpionate manner *via* the oxygen atoms of phosphoryl and carbonyl groups of the deprotonated substituent as well as the phosphoryl group oxygen atom of the non-deprotonated substituent (Fig. 5). The nitrate anion acts as bidentate ligand to lanthanide atom. The coordination polyhedron of lanthanide atom can be interpreted as a distorted bicapped trigonal prism according to geometrical criteria proposed by Porai-Koshits and Aslanov (coordination number 8) (Table S4†) in the both complexes (Fig. 6).[18] According to the SHAPE program data most likely the coordination polyhedron is between bicapped trigonal prism (C_{2v}), square antiprism (D_{4d}) and triangular dodecahedron (D_{2d}) (Table S5†).[19] The Ln–O bond lengths vary within 2.307(7) ÷ 2.525(5) Å in the coordination polyhedron (Table S2†).

The conformation of deprotonated $\mathbf{HL^-}$ ligand is very close to one in the sodium polymeric complex in the both lanthanide complexes. The N–H⋯N/O bifurcated intramolecular bonds are revealed in the both ligands between the neutral and deprotonated substituents in the $[\mathbf{Ln(HL)_2(NO_3)}]\cdot$i-PrOH complexes (Table S3†).

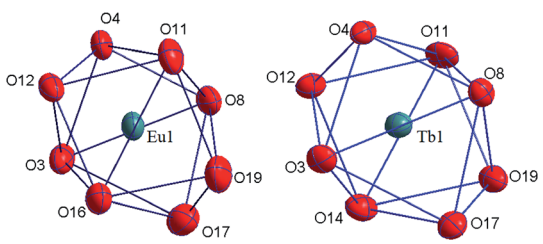

Fig. 6 The coordination polyhedron of Ln1 (Ln = Eu^{3+}, Tb^{3+}).

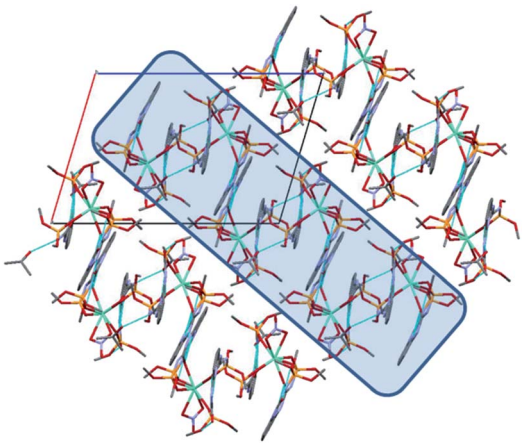

Fig. 7 The crystal packing of $[Ln(HL)_2NO_3]\cdot$i-PrOH, projection along the *b* crystallographic direction. H-atoms are omitted for clarity.

In the crystal phase, the $[Ln(HL)_2(NO_3)]$ and i-PrOH solvate molecules form the layers parallel to the (−101) crystallographic plane. The coordination complex and solvate molecules are bind by the N–H···O and O–H···N intermolecular hydrogen bonds (Table S3†) and (Fig. 7).

Hirshfeld surface analysis and fingerprint plots

Hirshfeld surface analysis is an effective tool for exploring packing modes and intermolecular interactions in molecular crystals, as they provide a visual picture of intermolecular interactions and of molecular shapes in a crystalline environment. Surface features characteristic of different types of intermolecular interactions can be identified, and these features can be revealed by color coding distances from the surface to the nearest atom exterior (d_e plots) or interior (d_i plots) to the surface. This gives a visual picture of different types of interactions present, and also reflects their relative contributions from molecule to molecule. Further, 2D fingerprint plots (FP), in particular the breakdown of FP into specific atom···atom contacts in a crystal, provide a quantitative idea of the types of intermolecular contacts experienced by molecules in the bulk and presents this information in a convenient color plot.

Hirshfeld surfaces comprising d_{norm} surface plots and FP were generated and analyzed for the crystal of **H_2L**, **NaHL**·i-PrOH, $[Tb(HL)_2(NO_3)]\cdot$i-PrOH, $[Eu(HL)_2(NO_3)]\cdot$i-PrOH in order to explore their packing modes and intermolecular interactions. The d_{norm} surfaces of molecules are shown in Fig. 8, and the FP for the overall contacts and individual atom···atom contacts in compounds synthesized are shown in Fig. 9. The dark-red spots on the d_{norm} surface arise as a result of the short interatomic contacts, *i.e.*, strong hydrogen bonds, while the intermolecular interactions appear as light-red spots. The analysis of the d_{norm} surface and FP gives a pictorial conformation (both qualitatively as well as quantitatively) to the nature and geometries of the hydrogen bonds and intermolecular interactions described in the crystal structure of the compounds.

The d_{norm} and FP are consistent with the observed intermolecular interactions. The light red spots on the d_{norm} surface located near the oxygen, nitrogen atoms and NH group (Fig. 8) can be attributed to the N···H and O···H contacts displayed in **H_2L**, **NaHL**·i-PrOH, $[Tb(HL)_2(NO_3)]\cdot$i-PrOH, $[Eu(HL)_2(NO_3)]\cdot$i-PrOH molecules.

The analysis of the fingerprint plots (Fig. 9) shows that the major contribution to the Hirshfeld surface is from H···H contact, with a contribution 39.2% for **H_2L**, 51.7% for **NaHL**·i-PrOH, 48.9% for $[Tb(HL)_2(NO_3)]\cdot$i-PrOH and 50.2% for $[Eu(HL)_2(NO_3)]\cdot$i-PrOH, the closest H···H contact occurs at d_i + d_e is a little over 1 Å. The contribution of H···H interactions

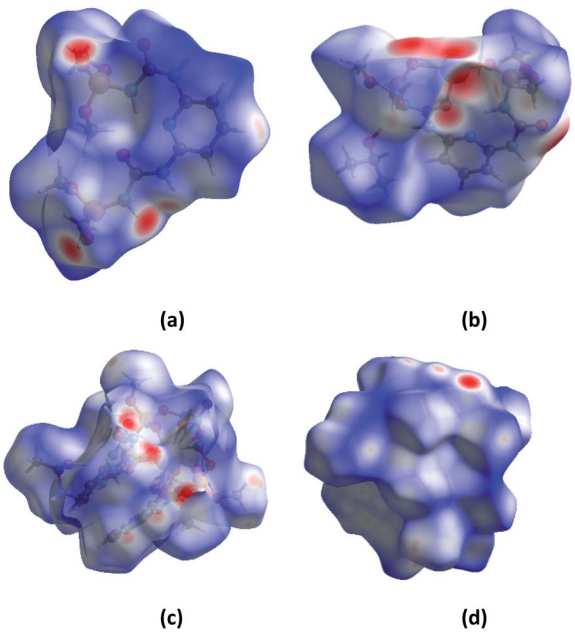

Fig. 8 The d_{norm} surfaces of molecules of H_2L (a), NaHL·i-PrOH (b), $[Tb(HL)_2NO_3]\cdot$i-PrOH (c), $[Eu(HL)_2NO_3]\cdot$i-PrOH (d).

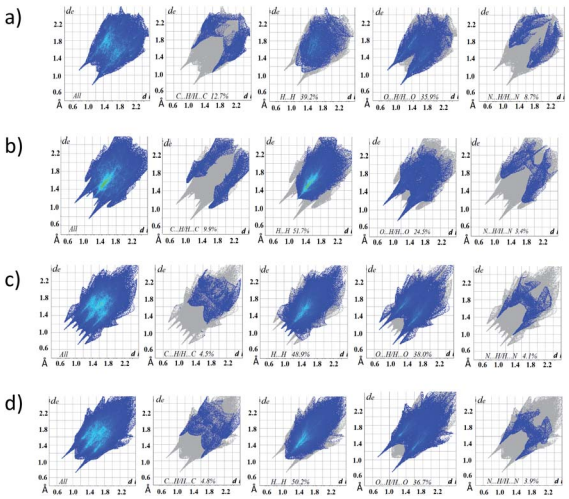

Fig. 9 The full two-dimensional fingerprint plot and fingerprint plots delineated into C···H/H···C, H···H, O···H/H···O and N···H/H···N contacts for H_2L (a), NaHL·i-PrOH (b), $[Tb(HL)_2(NO_3)]\cdot$i-PrOH (c), $[Eu(HL)_2(NO_3)]\cdot$i-PrOH (d).

Table 1 Contributions to intermoleculars interaction in percents

	H–H	O–H	N–H	C–H
H_2L	39.2	35.9	8.7	12.7
NaHL·i-PrOH	51.7	24.5	3.4	9.9
$[Tb(HL)_2NO_3]$·i-PrOH	48.9	38.0	4.1	4.5
$[Eu(HL)_2NO_3]$·i-PrOH	50.2	36.7	3.9	4.8

increases when comparing **H_2L** with sodium salt and lanthanide complexes, which can be explained by a change in the conformation of ligands when coordinated to metal ions and by the fact that the number of oxygen atoms capable of participating in intermolecular interactions due to coordination with the central atom decreases.

These findings are supported by an analysis of the second largest contribution comes from the closest O···H contact, with a 35.9% for **H_2L**, 24.5% for **NaHL**·i-PrOH, 38.0% for **$[Tb(HL)_2(NO_3)]$**·i-PrOH and 36.7% for **$[Eu(HL)_2(NO_3)]$**·i-PrOH. Where the decrease in the value for **NaHL**·i-PrOH when compared with **H_2L** is due to a change in the conformation of the molecule and the screening of coordinated oxygen atoms from intermolecular interactions and an inverse increase for **$[Tb(HL)_2(NO_3)]$**·i-PrOH and **$[Eu(HL)_2(NO_3)]$**·i-PrOH due to the presence of three oxygen atoms of nitrate groups in their composition. The contributions of N···H and C···H of intermolecular interactions naturally decrease when comparing **H_2L** with sodium salt and lanthanide complexes, the contributions of H···H increase, while the contributions of N···H and C···H decrease (Table 1).

Thus, the Hirshfeld surface and FP analysis give conclusive evidence, both qualitatively and quantitatively, of the various hydrogen bonds/intermolecular interactions displayed in the crystal structure.

Thermal gravimetric analyses

The thermal stability is an important feature that determines the possibility of compound practical applications. The thermal stability of the ligand and terbium coordination compound has been investigated using TGA in the temperature range of 20–600 °C (Fig. 10 and Fig. 11). According to the TGA curve (Fig. 10) for **H_2L** there is no obvious weight loss of up to 150 °C. If heated above 150 °C, the sample melts (endothermic effect at 176 °C) with simultaneous decomposition accompanied by weight loss near 6% and upon further heating decomposes abruptly. The decomposition is accompanied by one exothermic effect at 203 °C and two endothermic effects at 400 and 495 °C. The total weight loss after heating of the sample to 600 °C is 58%, and at the boundary value of the experimental temperature, the mass of the sample has not reached a constant value.

From the TGA data for the terbium complex one can conclude that significant weight loss occurs in one step (Fig. 11). Up to 180 °C there is a slight (~4.3%) loss of mass accompanied by endothermic effect, which may be due to evaporation of solvent. When heated above 180 °C, the compound begins to decompose. Considerable weight loss continues to a temperature of ~500 °C. The total weight loss is 42.3% and at the boundary value of the experimental temperature, the mass of the sample has not reached a constant value.

The decomposition of the complex is an endothermic process. The DTA curve shows an endothermic effect at a temperature of 244 °C.

Analysis of the IR spectrum of the solid residual in the crucible after TGA investigation reveals the formation of a mixture of terbium(III) orthophosphate and metaphosphate.

ESI-MS spectrometry

Analysis of the ESI-MS spectra of **H_2L** showed the formation of monomeric and oligomeric species $\{[\mathbf{H_2L}] + H^+\}^+$ (*m*/*z* 412.08), $\{[(\mathbf{H_2L})_2] + Na^+\}^+$ (*m*/*z* 845.14), $\{[(\mathbf{H_2L})_3] + Na^+\}^+$ (*m*/*z* 1256.22) (Fig. S1†).

Complex formation and the compositions of species formed in solution upon mixing **H_2L** ligand with Eu^{3+} and Tb^{3+} ions were first monitored using ESI-MS. Although this technique is not able to distinguish the ionizable protons in the species, the method can be successfully applied to determine the metal-to-ligand stoichiometry directly from the *m*/*z* values and has been used successfully by us when previously describing analogous systems.[20] Analysis of the ESI-MS spectra

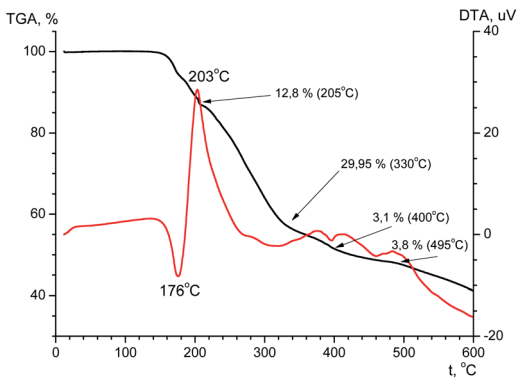

Fig. 10 The DTA (red line) and TGA (black line) weight loss trace for H_2L.

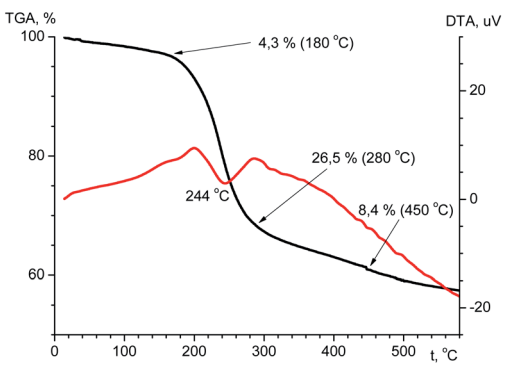

Fig. 11 The DTA (red line) and TGA (black line) weight loss trace for $[Tb(HL)_2(NO_3)]$·i-PrOH.

Table 2 The protonation constants of H_2L ligand[a]

Species	log β	log K
$[LH]^-$	9.07(1)	9.07
LH_2	16.85(2)	7.77
$[LH_3]^+$	19.14(3)	2.29

[a] 25 °C, $I = 0.1$ M NaCl.

of the reaction mixture of Eu^{3+} : **H_2L**, with a metal-to-ligand molar ratio 1 : 1, showed the formation of monomeric and oligomeric species successfully attributed to mononuclear, $[Eu(HL) + Cl^-]^+$ (m/z 597.96), $[Eu[(HL)_2]^{2-}]^+$(m/z 973.06), $[Eu[(HL)_2]^{2-}(\mathbf{H_2L})]^+$($m/z$ 1384.14), and dinuclear $[Eu_2[(L)_2]^{2-} + Cl^-]^+$($m/z$ 1156.94), species (Fig. S2†). It seems that the multinuclear complexes are adducts that arise during ESI-MS experiments; additional ESI-MS experiments showed that the multinuclear species are not resistant to the application of an increased SID voltage. All peak assignments were based on the comparison between the calculated and experimental isotope patterns (Fig. S2†).

ESI-MS spectra of the Tb^{3+}-**H_2L** is dominated by the signal corresponding to the $[Tb[(HL)_2]^{2-}]^+$ (m/z 979.06) complex (Fig. S2†). Additionally, in the spectra there are signals corresponding to mononuclear $[Tb(HL) + Cl^-]^+$ (m/z 603.96), and $[Tb[(HL)_2]^{2-}(\mathbf{H_2L})]^+$($m/z$ 1390.13) species.

Acid–base properties of the ligand

To evaluate the coordination capabilities of the ligand toward lanthanide ions, first the acid–base properties of **H_2L** were determined. The deprotonated form of the ligand, $[L^{2-}]$, may attach three protons in the measured pH range, two amide nitrogens and pyridine nitrogen. The protonation constants determined are presented in Table 2 (Fig. S3†). The first constant ($\log K_1 = 9.07$) corresponds probably to the protonation of amide NH group near the phosphorous atom of one arm of the ligand, the second ($\log K_2 = 7.77$) corresponds to the protonation of the same amide group of the second arm. As it was observed for one-arm analogous ligand, deprotonation of amide group located between carbonyl and phosphoryl group is preferable to another one.[21] The third ($\log K_3 = 2.29$) relates to the protonation of pyridine N atom. Low value of protonation constant of pyridine nitrogen atom, compared to similar systems,[22] may contribute to the formation of its intramolecular hydrogen bonds with N–H and may be influenced by an inductive effect of two arms and the possibility of formation of bifurcate hydrogen bonds.[23]

Table 3 Complex formation constants (log β) of the Eu^{3+} and Tb^{3+} complexes with H_2L[a]

	Eu^{3+}		Tb^{3+}	
Species	log β	log K	log β	log K
1 : 1				
$[MLH]^{2+}$	12.79(4)	—	12.40(7)	—
$[ML]^+$	4.90(2)	7.89	5.26(2)	7.14
$[ML_{-1}]$	−3.20(2)	8.10	—	—
$[ML_{-2}]^-$	−11.21(2)	8.01	−10.22(3)	—
$[ML_{-3}]^{2-}$	−20.25(3)	9.04	—	—
1 : 3				
$[MLH]^{2+}$	12.83(4)	—	13.30(4)	—
$[MLH_{-2}]^-$	−11.53(2)	—	−10.12(2)	—
$[MLH_{-3}]^{2-}$	−20.63(2)	9.10	−18.78(2)	8.66
$[M(LH)_2]^+$	25.08(3)	—	25.57(5)	—
$[ML_2H]$	17.40(3)	7.68	18.29(3)	7.28
$[ML_2]^-$	9.00(2)	8.40	10.26(3)	8.03

[a] 25 °C, $I = 0.1$ M NaCl.

Potentiometric titrations of Ln^{3+} complexes (Ln = Eu, Tb)

The stability constants and stoichiometry of the complexes obtained upon potentiometric titration of Eu^{3+} and Tb^{3+} with **H_2L** performed with metal-to-ligand molar ratio of 1 : 1 and 1 : 3 are listed in Table 3.

The data obtained for the Eu^{3+}/**H_2L** system with metal-to-ligand molar ratio of 1 : 1 suggest the formation of five species of stoichiometry 1 : 1 with different protonation state: $[EuLH]^{2+}$, $[EuL]^+$, $[EuLH_{-1}]$, $[EuLH_{-2}]^-$ and $[EuLH_{-3}]^{2-}$. The complexation process starts at pH 4 with the formation of the $[EuLH]^{2+}$ species (Fig. 12a) in which, amide group of one arm of ligand is still protonated. The log K_s values for the deprotonation reaction of the $[EuLH]^{2+}$ to $[EuLH_{-3}]^{2-}$ range from 7.89 to 9.04 and taking into account fact that in the bis-complexes (*vide infra*) amide group of only one arm of ligand is deprotonated one can suppose that described here deprotonation steps are probably associated with the deprotonation of metal coordinated water molecules to complete the coordination sphere of Eu^{3+} ions. The calculated log K_s lay in the range typical for the deprotonation of water molecule coordinated to lanthanide ions.[24] When the excess of ligand was used, the simultaneous formation of complexes with 1 : 1 and 1 : 2 metal-to-ligand stoichiometry was observed. As it was earlier, the coordination process starts with the formation of the $[EuLH]^{2+}$ species at pH around 4 (Fig. 12b). Due to the formation of bis-complexes starting from pH 6 it is not possible to detect all of the complexes of stoichiometry 1 : 1, as it was for the first system. In the first complex of stoichiometry 1 : 2, $[Eu(LH)_2]^+$, amide groups of one arm in both ligands are still protonated. As it is observed in the crystal structure of **$[Eu(HL)_2(NO_3)]\cdot$**i-PrOH, the coordination of Eu^{3+} ion proceeds through the two oxygen atoms ($O_{carbonyl}$, $O_{phosphoryl}$) of the deprotonated arm and monodentaly *via* $O_{phosphoryl}$ of the second arm of each ligand. The next deprotonation steps leading to the formation of $[ML_2H]$ and $[ML_2]^-$ species are probably related to the deprotonation of two water molecules coordinated to the Eu^{3+} ion, in place of NO_3^- present in the crystal structure.

For the Tb^{3+}/**H_2L** system very similar behavior was observed. The best fitting of the potentiometric experimental and calculated curves for metal-to-ligand molar ratio of 1 : 1 was obtained for the model containing complexes of 1 : 1

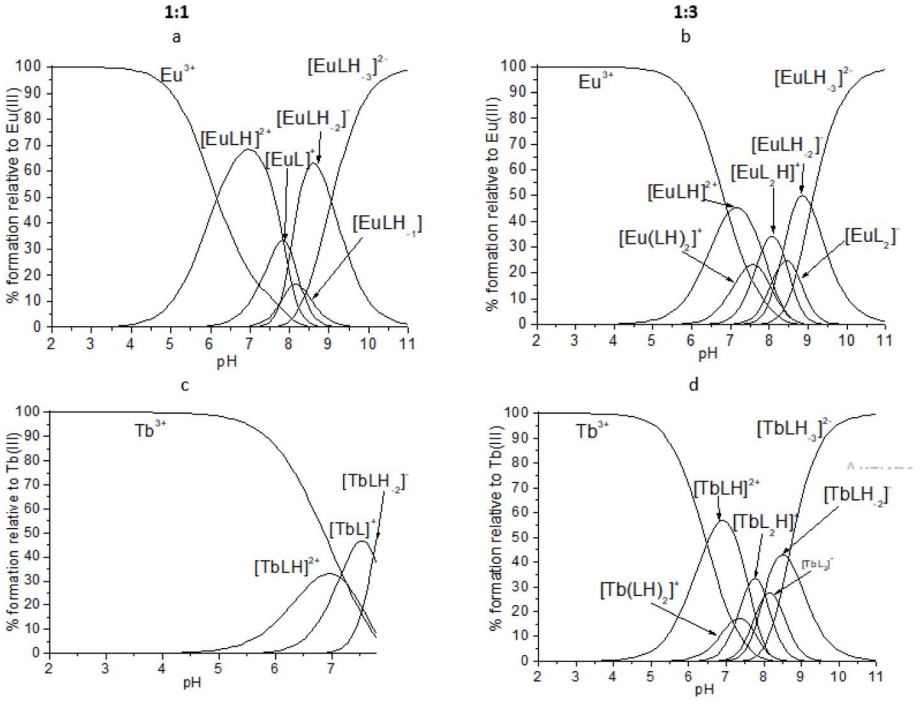

Fig. 12 Representative distribution diagrams for the systems Eu^{3+}/ (a and b) H_2L and Tb^{3+}/ (c and d)H_2L. Metal-to-ligand ratio of 1 : 1 and 1 : 3, [L] = 2 mM, I = 0.1 M NaCl.

stoichiometry with different protonation state (Fig. 12c). Unfortunately, above pH 7.7 precipitation was observed. Calculated model and distribution diagram calculated for the titration with the excess of the ligand is identical as for Eu^{3+} system (Table 3, Fig. 12d).

Conclusions

New bis-chelating carbacylamidophosphate (CAPh) ligand **H_2L** and its monodeprotonated sodium salt **NaHL** have been synthesized and characterized for the first time. The novel coordination compounds **$[Ln(HL)_2NO_3]$**·i-PrOH of europium and terbium have been obtained and their structural, IR spectral and thermal properties have been characterized. The protonation constants of **H_2L** and stability constants of Eu^{3+} and Tb^{3+} complexes with **H_2L** have been determined. It was shown that the coordination process starts with the formation of the $[LnLH]^{2+}$ species at pH around 4.

X-ray structural studies of the compounds obtained showed that the **H_2L** molecule has a monomeric structure and in crystals **H_2L** molecules are bonded in the chain *via* intermolecular hydrogen bonds through the P(O) group and the hydrogens of NH groups. Sodium salt **NaHL** in the crystal state has a dimer structure, which is realized due to the bridge function of the oxygen atoms of the PO of the deprotonated arm of CAPh ligand. The deprotonated chelate core is coordinated to the sodium ion in the bidentate manner *via* the oxygen atoms of the carbonyl and phosphoryl groups. The undeprotonated ligand arm is coordinated to the sodium ion in a monodentate manner through the oxygen atom of the P(O) group.

The coordination compounds **$[Eu(HL)_2(NO_3)]$**·i-PrOH and **$[Tb(HL)_2(NO_3)]$**·i-PrOH are isostructural and have a monomeric structure. Nitrate anion is coordinated to the lanthanide ion in the bidentate manner supplementing the coordination number of the lanthanide ion to 8. The structure of the coordination polyhedron of lanthanide ion can be interpreted as a distorted bicapped trigonal prism. There are numerous weak intermolecular and intramolecular contacts in the crystalline structure of all the compounds obtained.

The thermal properties of the complexes synthesized are investigated and their high thermal stability is shown (the decay start is about 200 °C), which indicates the prospect of the complexes for practical use in electroluminescent diode technology. And good solubility of the obtained complexes in water opens prospective for their practical application in biology and medicine.

Conflicts of interest

There are no conflicts to declare.

Acknowledgements

Funding sources: this work was supported by the Ministry of Education and Science of Ukraine (Project no. 19BF037-05) and Ministry of Science and Higher Education of Poland (research subsidy ZB2A-2020). The publication contains the results of studies conducted by President's of Ukraine grant for competitive projects (Project no. 19BF037-06).

References

1 (*a*) J.-C. G. Bünzli, *Chem. Rev.*, 2010, **110**(5), 2729–2755; (*b*) J.-C. G. Bunzli, *Handbook on the Physics and Chemistry of Rare Earths*, 2016, vol. 50, pp. 141–176; (*c*) G. Aromı and R. Olivier, *Handbook on the Physics and Chemistry of Rare Earths*, 2019, vol. 56, pp. 1–54.

2 (*a*) J. Kido and Y. Okamoto, *Chem. Rev.*, 2002, **102**, 2357–2368; (*b*) G. F. De Sa, O. L. Malta, C. De Mello Donega, A. M. Simas, R. L. Longo, P. A. Santa-Cruz and E. F. Da Silva, *Coord. Chem. Rev.*, 2000, **196**, 165; (*c*) K. Binnemans, *Chem. Rev.*, 2009, **109**, 4283.

3 H. Ur. Rashid and K. Yu, *J. Struct. Chem.*, 2013, **54**(1), 223–249.

4 B. H. Bakker, M. Goes, N. Hoebe, *et al.*, *Coord. Chem. Rev.*, 2000, **208**(1), 3–16.

5 F. Zinna, M. Pasini, F. Galeotti, C. Botta, L. DiBari and U. Giovanella, *Adv. Funct. Mater.*, 2016, **27**(1), 1603719.

6 (*a*) A. N. Gusev, M. Hasegawa, T. Shimizu, T. Fukawa, S. Sakurai, G. A. Nishchymenko, V. F. Shul'gin, S. B. Meshkova and W. Linert, *Inorg. Chim. Acta*, 2013, **406**, 279–284; (*b*) J. Shi, Y. Hou, W. Chu, X. Shi, H. Gu, B. Wang and Z. Sun, *Inorg. Chem.*, 2013, **52**(9), 5013–5022.

7 (*a*) P. Gawryszewska and P. Smolenski, *Ligands. Synthesis, Characterization and Role in Biotechnology*, Nova Science Publishers, 2014, p. 295; (*b*) O. O. Litsis, I. O. Shatrava, O. V. Amirkhanov, V. A. Ovchynnikov, T. Y. Sliva, S. V. Shishkina, V. V. Dyakonenko, O. V. Shishkin and V. M. Amirkhanov, *Struct. Chem.*, 2016, **27**(1), 341–355.

8 (*a*) N. Sayyadi, A. Care, R. E. Connally, A. C. Try, P. L. Bergquist and A. Sunna, *Sci. Rep.*, 2016, **6**(1), 27564; (*b*) H. F. Li, G. M. Li, P. Chen, W. B. Sun and P. F. Yan, *Spectrochim. Acta, Part A*, 2012, **97**, 197–201.

9 K. Binnemans, Rare-Earth Beta-Diketonates, in *Handbook on the Physics and Chemistry of Rare Earths*, ed. Gschneidner K. A. Jr, Bünzli J.-C. G. and Pecharsky V. K., Elsavier, Amsterdam, 2005, pp. 107–272.

10 (*a*) S. Trofimenko, *Scorpionates. The Coordination Chemistry of Polypyrazolylborate Ligands,* Imperial College Press, London, 1999; (*b*) C. Pettinari, *Scorpionates II: Chelating Borate Ligands*, Imperial College Press, London, 2008.

11 M. Bortoluzzia, G. Paoluccia, S. Polizzia, L. Bellottoa, F. Enrichib, S. Ciorba and B. S. Richards, *Inorg. Chem. Commun.*, 2011, **14**, 1762.

12 (*a*) G. M. Sheldrick, *Acta Crystallogr., Sect. A: Found. Adv.*, 2015, **71**, 3–8; (*b*) G. M. Sheldrick, *Acta Crystallogr., Sect. A: Found. Crystallogr.*, 2008, **64**, 112–122.

13 G. Gran, *Acta Chem. Scand.*, 1950, **4**(4), 559–577.

14 P. Gans, A. Sabatini and A. Vacca, *J. Chem. Soc., Dalton Trans.*, 1985, (6), 1195–1200.

15 L. Alderighi, P. Gans, A. Ienco, D. Peters, A. Sabatini and A. Vacca, *Coord. Chem. Rev.*, 1999, **184**, 311–318.

16 S. K. Wolff, D. J. Grimwood, J. J. McKinnon, M. J. Turner, D. Jayatilaka and M. A. Spackman, *Crystal Explorer 3.0*. University of Western Australia, Perth, 2012.

17 M. A. Spackman and D. Jayatilaka, *CrystEngComm*, 2009, **11**, 19–32.

18 M. A. Porai-Koshits and L. A. Aslanov, *J. Struct. Chem.*, 1972, **13**, 244–253.

19 *SHAPE v2.1, Continuous Shape Measures Calculation, 2013 Electronic Structure Group*, Universitat de Barcelona, contact: llunell@ub.edu.

20 I. O. Shatrava, V. A. Ovchynnikov, K. E. Gubina, T. Yu. Sliva, O. V. Severinovskaya, A. G. Grebenyuk, S. V. Shishkina and V. M. Amirkhanov, *Polyhedron*, 2018, **139**, 98–106.

21 I. Shatrava, V. Ovchynnikov, K. Gubina, S. Shishkina, O. Shishkin and V. Amirkhanov, *Struct. Chem.*, 2016, **27**(5), 1413–1425.

22 J. Gałęzowska, P. Kafarski, H. Kozłowski, P. Młynarz, V. M. Nurchi and T. Pivetta, *Inorg. Chim. Acta*, 2009, **362**, 707–713.

23 E. Gumienna-Kontecka, I. A. Golenya, A. Szebesczyk, M. Haukka, R. Krämer and I. O. Fritsky, *Inorg. Chem.*, 2013, **52**(13), 7633–7644.

24 J. Gałęzowska, R. Janicki, A. Mondry, R. Burgada, T. Bailly, M. Lecouvey and H. Kozłowski, *Dalton Trans.*, 2006, **36**, 4384–4394.

